

# Multiphysics modeling and simulations for Y-90 liver radioembolization

Emilie Roncali<sup>1,2</sup>, Carlos A. Ruvalcaba<sup>1</sup>, and Gustavo C.A. Costa<sup>1</sup>

<sup>1</sup>Department of Biomedical Engineering, University of California Davis, Davis , USA

<sup>2</sup>Department of Radiology, University of California Davis, Davis , USA

**Abstract.** Yttrium-90 (<sup>90</sup>Y) radioembolization is a form of liver cancer therapy where radioactive microspheres are injected into the liver arterial bloodstream via a catheter, delivering localized radiation to the tumor cells. Studies have shown a strong correlation between the administered dose and patient outcomes, highlighting the importance of accurate dosimetry in treatment planning.

However, current standard-of-care dosimetry practices in liver radioembolization rely on generic models that do not accurately consider individual patient anatomy, vasculature, and tumor burden. To address this limitation, we present an approach involving computational fluid dynamics (CFD) and Monte Carlo simulation developed at UC Davis. Patient cone-beam CT (CBCT) images are collected to extract the liver vasculature, which is then used to simulate the blood and microsphere transport through CFD in OpenFOAM. The volumetric distribution of microspheres and <sup>90</sup>Y absorbed dose distribution in the liver is then computed with the Geant4-based application GATE. The pre-treatment absorbed dose calculations aim at determining the optimal dose distribution for personalized treatment planning.

This abstract outlines ongoing investigations to develop a personalized dosimetry approach using CFDose improving the model fidelity and validating it against clinical <sup>90</sup>Y PET.

## 1 Introduction

Yttrium-90 (<sup>90</sup>Y) radioembolization is an internal radiation therapy to treat liver cancer (primary or metastatic), using microspheres 20-60  $\mu$ m in diameter loaded with <sup>90</sup>Y. The <sup>90</sup>Y microspheres are injected selectively into the liver arterial bloodstream through a catheter to deliver localized radiation. <sup>90</sup>Y represented more than 10,000 interventions in the US in 2022 [1]; multiple studies have shown a clear correlation between the tumor dose and patient outcome, which indicates that dosimetry should be considered in treatment planning. However, standard-of-care dosimetry remains simplistic, based on generic models in which a simple scaling factor is used to compute the absorbed dose distribution from <sup>90</sup>Y activity [2]. This model does not account for the patient's unique anatomy, vasculature, and tumor burden. Due to the intricacy between blood flow, microsphere transport in the liver vasculature, and radiation physics, multi-physics computational methods are well-suited to achieve accurate radioembolization dosimetry [3]. This abstract presents our current efforts in combining computational fluid dynamics (CFD) and Monte Carlo simulation to develop personalized dosimetry informed with patient imaging. We collect patient cone-beam CT (CBCT) images to extract the liver vasculature, in which we simulate the blood and microsphere transport using CFD in OpenFOAM [4]. This provides the microsphere volumetric distribution and <sup>90</sup>Y activity distribution which in turn is used to compute the absorbed dose with Geant4 Application for Tomographic Emission (GATE) [5]. Our goal is to create a liver digital twin for radioembolization treatment planning, in which the digital

twin is used to compute the optimal dose distribution. We

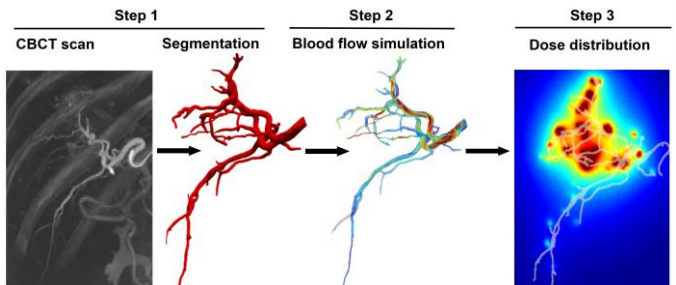


Figure 1. CFDose. 1) Hepatic artery segmentation from CBCT. 2) CFD simulation. 3) Simulated radiation dose distribution.

called this liver model CFDose [3].

## 2 Materials and Methods

### 2.1 Patient data and image processing

In CFDose, personalization is achieved by using each patient's angiogram to create the vascular mesh to carry out the CFD simulation. The CBCT acquired during treatment planning was segmented with a piece-wise approach based on level sets in 3D Slicer and meshed with gmsh [6]. In the example shown in Figure 1, segmented vessels were as small as 0.45 mm in diameter, and 46 outlets were identified.

### 2.2 CFD simulation and multiscale model

To improve the precision of the microsphere simulation in small vessels, we modeled three phenomena that strongly direct the local microsphere deposition and were not previously considered in CFDose: blood is modeled as a non-Newtonian fluid, the catheter tip geometry and positioning extracted from patient scans (Figure 2), and discrete particle transport simulating microsphere dynamics. This new model included a 1-way coupling between the micro-

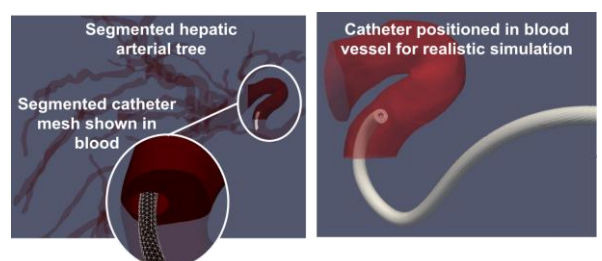


Figure 2. Catheter tip segmented, meshed, and shown with realistic positioning in blood flow.

spheres and the blood through discrete phase modeling to account for particle forces experienced by the microspheres during transport [7]. The model adequately captures the microsphere transport dynamically throughout the vasculature. Boundary conditions at the vessel wall are considered non-slip and non-deforming, while resistor-capacitor circuit analogs (known as 2- and 3-element

windkessel-type) are prescribed at the vasculature downstream from the simulation domain which is not resolved in the image-based CFD domain. The resistors were assumed to be equally distributed amongst outlets, for each liver segment.

### 2.3 Microsphere dose distribution with GATE

$^{90}\text{Y}$  is a  $\beta$ - emitter with a maximum energy of 2.28 MeV and a mean energy of 930 keV, corresponding to a maximum and mean electron range of 11 mm and 2.5 mm in water [8].

An isotropic dose point kernel with a 0.25 mm x 0.25 mm x 0.25 mm size was computed in GATE, using the  $^{90}\text{Y}$  energy spectrum calculated from the Fermi theory for beta decay (Figure 3).

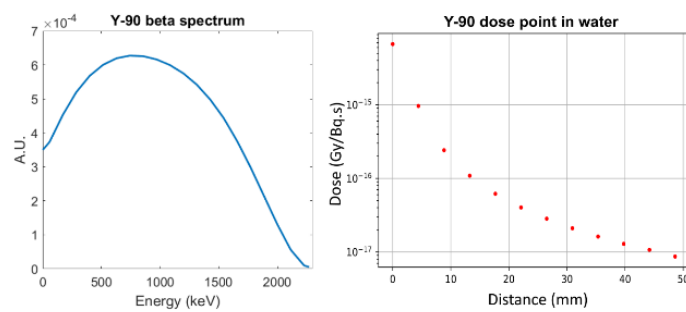


Figure 3. Left:  $^{90}\text{Y}$  beta spectrum (mean energy 930 keV). Right: Dose kernel profile showing a rapid decrease of deposition with distance (log scale).

The dose distribution was obtained by convolving the dose kernel with the microsphere distribution obtained from the CFD simulation or using a full Monte Carlo simulation [9].

### 2.4 Comparison with clinical dosimetry

Scans up to 60 minutes were acquired within 48 hours of treatment to image the  $^{90}\text{Y}$  activity with the total-body uEXPLORER scanner (United Imaging Health) for high quantitative accuracy at high resolution in a single bed position, using a protocol we previously validated [9]. The actual dose distribution was computed in the liver using the quantitative  $^{90}\text{Y}$  images, the patient CT, providing the closest measurement to ground truth [9]. All PET acquisitions were accompanied by a low-dose CT scan for attenuation correction and anatomical delineation. Partial volume correction was applied using a previously determined recovery coefficient [10].

## 3 Results

### 3.1 CFD simulations

CFD simulations including particle transport showed the asymmetry of the flow and distribution between vessels and the importance of considering the vessel tortuosity

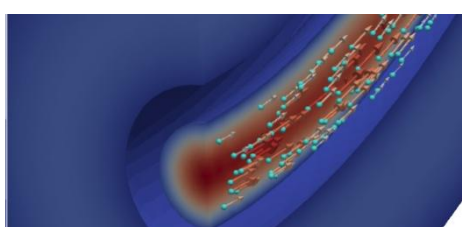


Figure 4. Illustration of skewed microsphere flow toward the vessel wall.

when developing the flow upstream of the inlet (Figure 4). [11]

Our most recent work has focused on modeling the catheter geometry and flow within the vessel, to fully account for its perturbation of the blood flow in which the injected microspheres blend.

### 3.2 Comparison between simulated dose distribution and clinical PET

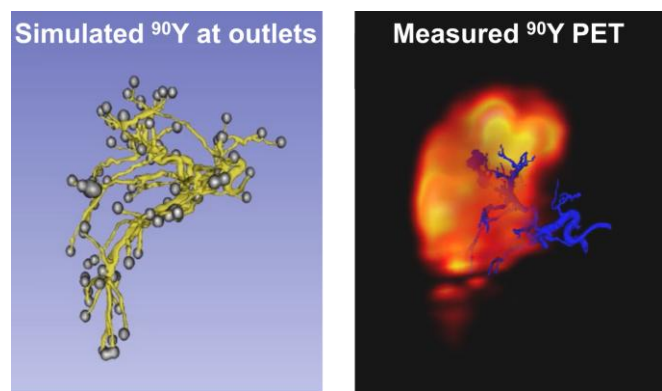


Figure 5. Left: Arterial tree segmented from CECT with predicted microsphere clusters at the outlets. Right: Clinical  $^{90}\text{Y}$  PET overlaid with the arterial tree.

We compared the liver dose distribution with a clinical  $^{90}\text{Y}$  PET scan acquired 1 h post treatment (Coronal view, Figure 5) and found that the predictive dosimetry was consistent with the activity mostly located in segments 7 and 8, as determined by a board-certified radiologist [3]. Figure 5 shows the 3D vascular mesh with clusters of microspheres simulated at each outlet. The cluster size is indicative of the number of microspheres. This encouraging first comparison indicates the accuracy of CFDose and shows the feasibility of validating CFD-based dosimetry with  $^{90}\text{Y}$  PET.

Next steps include voxelwise comparison of the simulated and measured distributions, adding motion correction to the clinical PET data, and developing the liver model.

## 4 Discussion and conclusion

We present our newest results on the development of CFDose, a computational vascular model of the liver that we plan to integrate into an optimization program to find the best activity and injection spot in  $^{90}\text{Y}$  radioembolization. Our next steps include personalization of the boundary conditions, which is an important part of transforming this model into a liver digital twin. While this model utilizes computationally intense CFD simulations, we plan to apply our expertise on generative adversarial networks (GANs) to speed up the computation and rapidly provide an estimated dose distribution.

## 5 References

- [1] BTG. "Package Insert TheraSphere® Yttrium-90 Glass Microspheres. Rev 14," 2016; <http://www.therasphere.com/>.
- [2] S. A. Gulec, G. Mesoloras, and M. Stabin, "Dosimetric Techniques in 90Y-Microsphere Therapy of Liver Cancer: The MIRD Equations for Dose Calculations," *J. Nucl. Med.*, vol. 47, no. 7, pp. 1209-1211, 2006.
- [3] E. Roncali, A. Taebi, C. Foster, and C. T. Vu, "Personalized Dosimetry for Liver Cancer Y-90 Radioembolization Using Computational Fluid Dynamics and Monte Carlo Simulation," *Ann. Biomed. Eng.*, vol. 48, pp. 1499-1510 2020.
- [4] C. Greenshields, *OpenFOAM v10 User Guide*, London, UK: The OpenFOAM Foundation, 2022.
- [5] D. Sarrut *et al.*, "A review of the use and potential of the GATE Monte Carlo simulation code for radiation therapy and dosimetry applications," *Med. Phys.*, vol. 41, no. 6, pp. 064301, 2014.
- [6] C. Geuzaine, and J. F. Remacle, "Gmsh: A 3- D finite element mesh generator with built- in pre- and post- processing facilities," *Numerical Meth Engineering*, vol. 79, no. 11, pp. 1309-1331, 2009.
- [7] E. M. Childress, and C. Kleinstreuer, "Impact of fluid-structure interaction on direct tumor-targeting in a representative hepatic artery system," *Ann Biomed Eng*, vol. 42, no. 3, pp. 461-74, 2014.
- [8] H. Ryde, P. Thieberger, and T. Alväger, "Two-Photon De-Excitation of the 0+ Level in Zr<sup>90</sup>," *Physical Review Letters*, vol. 6, no. 9, pp. 475-478, 1961.
- [9] G. C. A. Costa *et al.*, "Radioembolization Dosimetry with Total-Body Y-90 PET," *J. Nucl. Med.*, pp. jnumed.121.263145, 2021.
- [10] B. A. Spencer, N. Omidvari, G. Costa, M. Rusnak, D. T. Caudle, C. Foster, C. T. Vu, and E. Roncali, "Comparison Between EXPLORER Total-body PET with Conventional PET Imaging of Y-90 Radioembolization: A Phantom and Clinical Study," in IEEE Nuclear Science Symposium and Medical Imaging Conference 2020.
- [11] C. Ruvalcaba, A. Rajamani, and E. Roncali, "Characteristics of catheter injection for predictive particle transport modeling in Y-90 transarterial radioembolization procedures," *Bulletin of the American Physical Society*, vol. 11/21/2023, 2023.